JOURNAL OF Materials CHEMISTRY

The effect of cobalt on the structural properties and reducibility of CuCoZnAl layered double hydroxides and their thermally derived mixed oxides

S. Velu,* K. Suzuki,* S. Hashimoto, N. Satoh, F. Ohashi and S. Tomura

Ceramics Research Institute, National Institute of Advanced Industrial Science and Technology, Nagoya 462 8510, Japan. E-mail: k.suzuki@aist.go.jp; velu-subramani@aist.go.jp

Received 19th February 2001, Accepted 18th May 2001
First published as an Advance Article on the web 4th July 2001

A new series of CuCoZnAl layered double hydroxides (LDHs) with various Cu/Co atomic ratios were synthesized by a coprecipitation method at constant pH ≈ 9. The effects of Co on the structural properties and reducibility of both as-synthesized and calcined materials were investigated thoroughly by employing powder X-ray diffraction (XRD), ultraviolet–visible diffuse-reflectance spectroscopy (UV–Vis DRS), thermogravimetry–differential thermal analysis (TG–DTA), and temperature programmed reduction (TPR) methods. Characterization of as-synthesized materials using these techniques revealed the formation of well-crystallized hydrotalcite (HT)-like LDHs with a general formula $[Cu_{1-(x+y+z)}Co_xZn_yAl_z(OH)_2]^{z+}[(CO_3^{2-})_{z/2}\cdot mH_2O]^{z-}$ as a major phase. Thermal analyses of materials indicated three stages of endothermic weight loss processes due to the loss of interlayer water and some loosely bound CO_3^{2-} (100–250 °C), loss of structural water and CO_3^{2-} (250–400 °C) and the loss of some strongly held CO_3^{2-} anions (above 500 °C). The structural and redox properties of mixed oxides obtained upon thermal activation were investigated by calcining the LDH precursors at 300, 450, 700 and 900 °C. The Cu-rich sample generated a mixture of CuO, ZnO and $CuAl_2O_4$ spinel, while Co-based spinel phases were observed at all temperatures in the case of the Co-rich sample. Materials containing both Cu and Co showed a mixture of CuO, Co-based spinel and $CuAl_2O_4$ spinel. The interesting observation of the present study was that the reducibility of Cu^{2+} species of the CuO was enhanced with increasing Co content. On the other hand, the reducibility of Co species decreased with increasing Cu content.

Introduction

Layered double hydroxides (LDHs), also known as hydrotalcites (HTs) or anionic clays, are an important class of material currently receiving increasing interest owing to their potential applications in a variety of areas such as catalysis, adsorbents, ion exchangers and modified electrodes.[1–5] Very recently these materials have also been found to be useful in medicines as non–viral vectors.[6] The structure of LDH consists of positively charged brucite $[Mg(OH)_2]$-like M(II)–M(III) hydroxide layers, which are separated from each other by an interlayer composed of anions and water of crystallization. These compounds are represented by the general formula: $[M(II)_{1-x}M(III)_x(OH)_2]^{x+}[(A^{n-})_{x/n}\cdot mH_2O]^{x-}$, where M(II) is a divalent cation such as Mg, Cu, Ni, Co, Zn; M(III) is a trivalent cation such as Al, Fe, Cr, V, Mn, Ga, Rh; and A^{n-} is a charge compensating anion such as CO_3^{2-}, NO_3^-, Cl^-, polyoxometallates or other macrocyclic ligands.[1,4,5]

Thermal decomposition of LDHs around 400 °C leads to the formation of mixed metal oxides with some unique properties such as high metal dispersion, high-surface area, high thermal stability, *etc.*, which are essential for the material to function as a promising catalyst. Thus, a variety of commercial solid catalysts employed in various industrially important chemical processes are currently obtained *via* thermal decomposition of LDHs.[1,7–9] For instance, the mixed $CuO/ZnO/Al_2O_3$ oxide catalysts derived from LDH are found to be very active in methanol synthesis and water-gas shift (WGS) reactions.[1,10] These catalysts are also active and selective in the partial oxidation of methanol and steam reforming of methanol reactions.[8,11,12] We have recently reported the oxidative steam reforming of methanol as a new method for H_2 production over these CuZn-based catalysts.[13,14]

CuCo-based multi-component mixed oxides such as Cu/Co(Zn)/Al(Cr) derived from LDH precursors have been developed to convert synthesis gas ($CO/CO_2/H_2$) to methanol and higher alcohols.[1,15–18] They are also found to be active in CO oxidation, hydroxylation of phenol and oxidation of cresols, *etc.*[19,20] However, the physicochemical properties, particularly the nature of the crystalline phases formed and their reducibility, of these mixed oxide catalysts depend on the method of preparation and their thermal history.[16,17] Unfortunately, there are only a few reports in the literature on the synthesis and characterization of similar CuCo-based multimetallic LDH systems.[21–23] To the best of our knowledge no systematic study on the structural and redox properties of these interesting materials has been reported.

The aim of the present study is to investigate systematically the effect of Co on the nature of the crystalline phases formed and redox properties of CuCoZnAl-LDHs as well as the multicomponent mixed oxides obtained by thermal decomposition at various temperatures. These mixed oxides are currently being investigated as catalysts in the oxidative steam reforming of methanol for H_2 production.

Experimental

Synthesis of CuCoZnAl-LDHs

CuCoZnAl-LDHs with different Cu : Co atomic ratios were synthesized by a coprecipitation method at room temperature by reacting aqueous solutions containing a mixture of

Table 1 Chemical compositions and lattice parameters of CuCoZnAl-LDHs

	Chemical composition (atomic ratio)					Lattice parameters/Å	
Precursor	Cu	Co	Zn	Al	(Cu+Co+Zn)/Al	*a*	*c*
CuCoP-1	2.53	0.00	0.77	1	3.27	3.08	22.67
CuCoP-2	1.73	0.75	0.77	1	3.25	3.08	22.53
CuCoP-3	1.35	1.17	0.83	1	3.35	3.08	22.72
CuCoP-4	0.88	1.59	0.81	1	3.28	3.08	22.89
CuCoP-5	0.00	2.27	0.81	1	3.08	3.09	23.10

$M^{II}(NO_3)_2$ (M^{II} = Cu, Co, Zn) and $Al(NO_3)_3$ as precursors and a mixture of NaOH (≈2 M solution) and Na_2CO_3 (≈0.3 M solution) as precipitants at a constant pH (≈9).[12] The resulting precipitate was aged at 65 °C for 30 min under stirring in a magnetic stirrer then filtered off, washed with deionized water several times until the pH of the filtrate was 7 and then dried in an air oven at 70 °C overnight. The powders of the as-synthesized samples were calcined at 300, 450, 700 and 900 °C for 5 h in a muffle furnace (static air atmosphere) with a heating rate of 10 °C min^{-1}. The as-synthesized samples in the following sections will be represented as CuCoP-1 through CuCoP-5 while those calcined at 450 °C for 5 h will be referred to as CuCoC-1 through CuCoC-5.

Materials characterization

The chemical compositions of the as-synthesized samples were determined by X-ray fluorescence (XRF) spectroscopy (Shimadzu Co. Lab center, XRF-1700 sequential X-ray fluorescence spectrometer). The powder X-ray diffraction (XRD) patterns of the as-synthesized as well as calcined samples were obtained in the 2θ range 5–70° using a Rint 2100 model XRD instrument equipped with Ni-filtered Cu K_α radiation (λ = 1.5418 Å). The data were collected with a scan rate of 1° 2θ min^{-1}. Elemental Si was used to correct the observed interplanar '*d*' spacing. Simultaneous thermogravimetry and differential thermal analysis (TG-DTA) experiments were performed on a SSC/5200, SII Seiko instrument in the temperature range 50 to 700 °C in both N_2 and air atmospheres. A temperature ramp of 10 °C min^{-1} was employed. The ultraviolet–visible diffuse-reflectance spectra of all samples were recorded using a Perkin-Elmer UV–Vis Spectrometer coupled with a Labsphere RSA-PE-18 Reflectance Spectroscopy accessory. The samples were diluted (20 weight%) in $MgCO_3$ which was used as a reference in the present study. The spectra were recorded under ambient conditions and the data were automatically transferred according to the Kubelka–Munk equation: $f(R)=(1-R_\infty)^2/2R_\infty$. For the purpose of comparison, the spectra of reference samples namely CuO, Co_3O_4 (Wako Chemicals, Japan) were recorded. A reference sample of $CoAl_2O_4$ spinel was also prepared by a chelate gel method using citric acid as a chelating agent. Stoichiometric amounts of metallic Co (99.9%) and Al (99.99%) (molar ratio Co : Al = 1 : 2) were dissolved in nitric acid at 100 °C. Citric acid was added to this solution, and then the citrate amorphous precursor was obtained upon heating this mixed solution at 230 °C. The resulting citrate amorphous precursor was decomposed at 1000 °C for 24 h by which time a pure single phase $CoAl_2O_4$ spinel was obtained without any impurity. The reducibility of LDHs calcined at different temperatures was investigated by temperature-programmed reduction (TPR). The experimental parameters were selected to meet the recommendations of Monti and Baiker.[24] About 20 mg of the sample was placed in a quartz reactor 4 mm i.d.) and reduced in a stream of H_2 (5 vol.% in Ar) at a heating rate of 5 °C min^{-1} up to 800 °C or for a few cases up to 900 °C. The hydrogen consumption due to the reduction of Cu and Co cations was monitored continuously by a gas chromatograph (Shimadzu GC-8A) equipped with a thermal conductivity detector (TCD). The quantity of hydrogen consumed was determined from the TPR peak areas calibrated with a known amount of standard CuO sample (Wako Chemicals, Japan).

Results and discussion

As-synthesized CuCoZnAl-LDHs

X-Ray diffraction (XRD) and chemical analysis. The chemical composition and lattice parameters of CuCoZnAl-LDHs series synthesized in the present study are summarized in Table 1, while their XRD patterns are presented in Fig. 1. The Cu : Co atomic ratio in the gel was varied while keeping the Zn and Al atomic ratio constant. The XRD patterns of the materials are typical of the layered rhombohedral structure of hydrotalcite (HT)-like LDH (JCPDS file No. 37-629), which exhibits sharp and symmetric reflections at low 2θ angles and broad and asymmetric reflections at higher 2θ angles. The Co-free CuCoP-1 is highly crystalline and the crystallinity decreases with increasing Co content. However, CuCoP-1 is

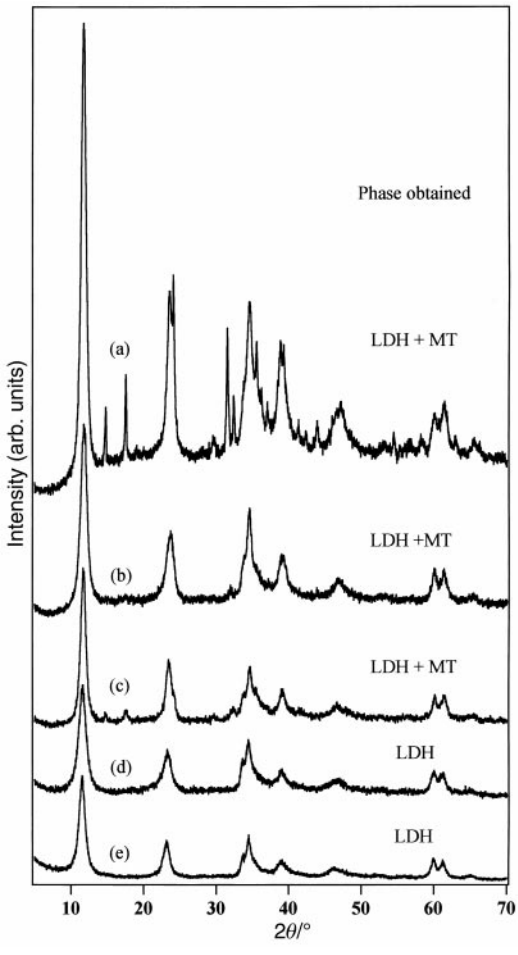

Fig. 1 X-Ray powder diffraction patterns of CuCoZnAl-LDHs: (a) CuCoP-1, (b) CuCoP-2, (c) CuCoP-3, (d) CuCoP-4 and (e) CuCoP-5. LDH = layered double hydroxide, MT = malchite.

accompanied by an impurity phase corresponding to malachite (MT), [$Cu_2CO_3(OH)_2$; JCPDS file No. 41-1390] because of the operation of the Jahn–Teller effect in Cu^{2+} ions in octahedral coordination.[1] The intensity of the MT peaks gradually decreases with decreasing Cu content or increasing Co content. The CoZnAl-LDH without Cu (CuCoP-5) exhibits a single phase corresponding to LDH. The lattice parameter '*a*' of these materials corresponds to the average cation–cation distance within the brucite-like layer and can be calculated as: $a = 2 \times d(110)$. On the other hand, the '*c*' parameter is related to the thickness of the brucite-like layer and the interlayer distance, and can be determined by averaging the '*d*' values of the (003) and (006) peaks using the formula: $c/3 = 1/2\{d(003) + [2 \times d(006)]\}$.[25] It can be seen that the '*a*' parameter remains almost constant, while the '*c*' parameter increases to a minor extent with increasing Co content in the sample. The observation of a constant '*a*' parameter with decreasing Cu content and concomitant increase in the Co content in the samples provides evidence that Co^{2+} cations substitute Cu^{2+} in the CuZnAl-LDH framework. This leads to the retention of the average cation–cation distance as the ionic radii of Cu^{2+} and Co^{2+} in octahedral coordination (high spin environment) are very similar (ionic radii of Cu^{2+}, Co^{2+}, Zn^{2+} and Al^{3+} in their octahedral coordination are 0.87, 0.88, 0.89, and 0.67 Å, respectively).[26] The results also imply that, under our preparation conditions, the Co^{2+} ions remain predominantly in the +2 state and are not oxidized to the +3 state as reported earlier.[27] Note that the ionic radii of Co^{2+} and Co^{3+} in high spin octahedral coordination are 0.88 and 0.75 Å, respectively.[26] Hence, in contrast to what was observed, a minor decrease in the '*a*' parameter with increasing Co content can be anticipated if some of the Co^{2+} is oxidized to Co^{3+} during the synthesis. Relatively lower values of the '*c*' parameter observed for the Cu-rich sample may be due to the presence of the MT impurity phase.

Ultraviolet–visible diffuse-reflectance spectroscopy (UV–Vis DRS). UV–Vis DRS was employed to understand the nature of coordination of metal ions in the LDH framework as well as in the mixed oxides obtained upon calcination at 450 °C. The spectra of CuCoP-1 without Co, CuCoP-3 containing both Cu and Co with a Cu/Co atomic ratio ≈ 1, and CuCoP-5 containing Co without Cu are shown in Fig. 2. For comparison, the spectra of reference oxide samples, namely CuO, $CoAl_2O_4$ and Co_3O_4, are also included in the inset of Fig. 2, while assignments of their band maxima are summarized in Table 2. The spectrum of CuCoP-1, which contains a well-crystallized LDH phase together with MT, exhibits a broad band in the region between 400 and 800 nm with maxima noticeable at *ca.* 480 and 700 nm. The latter band can be assigned to the ^2E_g (D) → $^2T_{2g}$ (D) transition of Cu^{2+} ions existing in an octahedral coordination in the LDH framework.[21] However, the broadness of the band suggests that the ions are significantly distorted from an octahedral environment. Thus, this band is the envelope of the $d_{z^2} \rightarrow d_{x^2-y^2}$, $d_{xz,\,yz} \rightarrow d_{x^2-y^2}$, and $d_{xy} \rightarrow d_{x^2-y^2}$ transitions that occur when Cu^{2+} ions are in a distorted

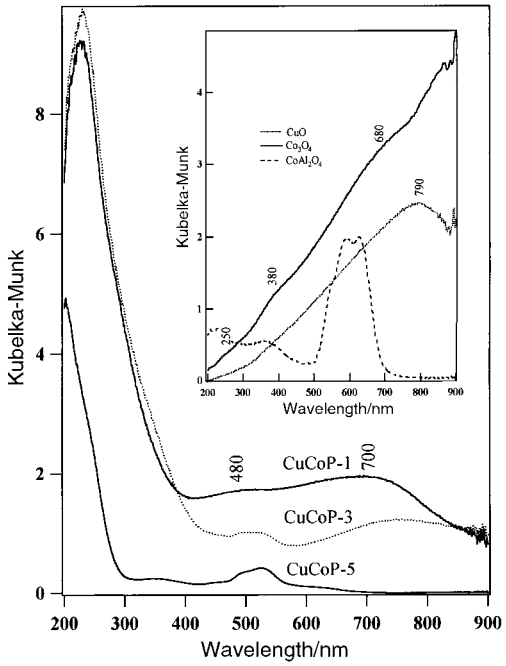

Fig. 2 Ultraviolet–visible diffuse reflectance spectra of CuCoZnAl-LDHs. The spectra of CuO, Co_3O_4 and $CoAl_2O_4$ reference samples are shown in the inset for comparison.

octahedral symmetry in the LDH precursor. The band at *ca.* 480 nm and a large band below 350 nm are due to the $O_2^{2-} \rightarrow Cu^{2+}$ ligand to metal charge transfer (LMCT) transitions.[14]

The Co-rich CuCoP-5 exhibits a weak and broad band around 500 nm. This band appears to be formed by two or three component bands with a maximum centered at *ca.* 520 nm. The position of this band is similar to that observed in the in the UV–visible spectrum of Co^{2+} octahedrally coordinated by weak-field ligands such $[Co(H_2O)_6]^{2+}$.[29] Hence, this band is assigned to the $^4T_{1g}$ (F) → $^4T_{1g}$ (P) transition of octahedrally coordinated Co^{2+} existing in the LDH framework. Ulibarri *et al.*[30] have also observed a similar band in the CoAl-LDH system and attributed it to octahedral Co^{2+} in the LDH framework. No band around 700 nm corresponding to octahedral Co^{3+} can be detected in our system, indicating that under our preparation conditions cobalt is present in the LDH matrix predominantly as Co^{2+}, which is in agreement with our XRD data. The large band below 300 nm is due to the LMCT transition.[21] The sample CuCoP-3, which contains both Cu^{2+} and Co^{2+}, exhibits bands in their respective regions similar to those observed in CuCoP-1 and CuCoP-5, indicating the existence of both of these cations in the LDH framework in octahedral coordination.

Thermogravimetry–differential thermal analysis (TG–DTA). The thermal stability of CuCoZnAl-LDHs was examined by simultaneous TG-TDA experiments. Since the materials contain oxidizable Co^{2+} cations, the TG-DTA

Table 2 Assignments of DRS band positions of some reference compounds in the present study

Compound	Band position/nm	Symmetry	Assignment	Reference
CuO	790	Cu^{2+} (oh)	^2E_g (D) → $^2T_{2g}$ (D)	21
$CoAl_2O_4$	Triplet between 550 and 650	Co^{2+} (td)	$^4A_2$ (F) → $^4T_1$ (P)	28
Co_3O_4	≈680	Co^{3+} (oh)	$^1A_{1g}$ (I) → $^1T_{1g}$ (I)	17, 21
	≈380	Co^{3+} (oh)	$^1A_{1g}$ (I) → $^1T_{2g}$ (I)	
	≈250	Co^{3+} (oh)	$O_2^{2-} \rightarrow Co^{3+}$ (LMCT)	

(oh) = Octahedral coordination; (td) = tetrahedral coordination; LMCT = ligand to metal charge transfer.

curves were recorded using both air as well as N_2 as carrier gases. For the sake of clarity, the differential curves of TG (DTG) are presented in Fig. 3. It is therefore convenient to compare the TG weight loss processes with those of the enthalpy changes occurring during the thermal transformations of LDHs in DTA (Fig. 4). The peak positions and the shape of both DTG and DTA curves recorded in air are slightly different, particularly for Co-rich samples, compared to those recorded in N_2, which may be attributed to the involvement of partial oxidation of Co^{2+} during thermal decomposition. Generally, the LDHs exhibit two major weight loss processes.[31] Based on the results obtained from combined TG and mass spectrometry studies, the first weight loss (T_1) below 200 °C has been assigned to the loss of interlayer water together with some loosely bound interlayer anions such as CO_3^{2-} as CO_2. The second weight loss (T_2) between 200 and 400 °C has been assigned to the loss of structural water and CO_2 upon destruction of the layered structure.[32] The temperatures of these two weight loss processes depend on several factors such as the nature of the cations and their compositions in the brucite-like layer, the nature of interlayer anions, the crystallinity of the materials, *etc.* It can be seen from the DTG patterns (Fig. 3) that the T_1 process occurs almost in the same temperature range, while the position of T_2 gradually shifts toward lower temperature with decreasing Cu content or increasing Co content in the sample. This indicates that the Co-containing LDHs are thermally less stable probably because of the presence of the oxidizable cation, Co^{2+}. In fact, the Co-containing LDHs lead to the corresponding spinel phases upon calcination above 200 °C (*vide infra*), while spinel phases can be obtained only above 700 °C in the LDH systems containing cations other than Co^{2+}. Another interesting feature noticed in the DTG traces is the appearance of a third weight loss (T_3) around 580 °C in the Cu-rich CuCoP-1 sample. The intensity of this peak gradually decreases and the peak position shifts toward lower temperature with decreasing Cu content. On the other hand, the T_3 peak is completely absent in the case of Co-rich CuCoP-5. Such a high temperature weight loss process has already been recorded by us[33] as well as by many other researchers exclusively in Cu-based LDH systems.[32,34] Our temperature programmed evolved gas analysis (EGA) of CuMnAl-LDHs indicated the release of CO_2 at this temperature.[33] We have attributed this feature to some type of reaction occurring between the brucite-like sheet and carbonate anions in the interlayer to form an "oxycarbonate" of chemical composition $[M^{II}M^{II}_xO_y(CO_3)_z]$, wherein the metal–oxygen bond remains intact and hence carbonate anions are substantially retained. This hypothesis has recently been confirmed by Rives and Kannan using FT-IR spectroscopy of the CuNiAl-LDH system.[34]

The peak positions and the shapes of the DTA curves shown in Fig. 4 are almost identical to those of the DTG curves in most of the cases. This implies that the weight loss processes occurring in TG (DTG) are associated with endothermic transformations observed in DTA. However, minor differences can be noticed, particularly in the traces for the Co-containing materials recorded in air. For instance, the DTG peak corresponding to T_2 in CuCoP-4 as well as in CuCoP-5 containing relatively large amounts of Co is very intense compared to the respective T_1 peaks, while the corresponding endothermic peaks in DTA are weak. In addition, a weak exothermic feature around 330 °C can be seen in these samples.

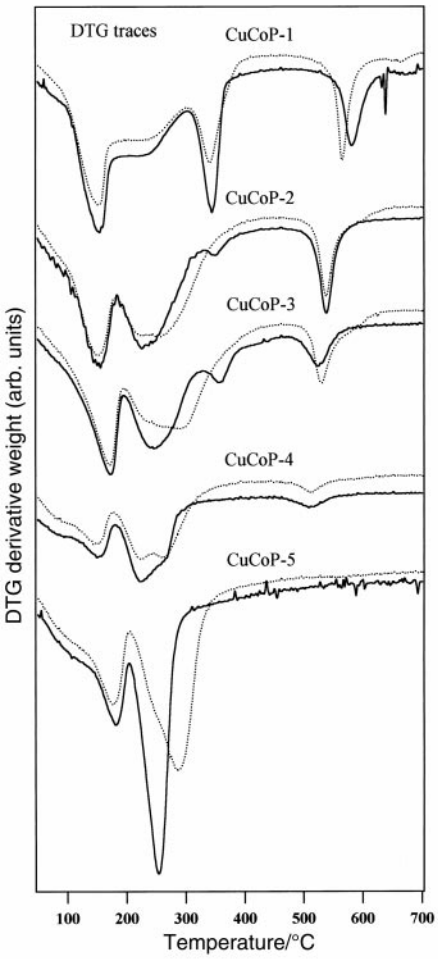

Fig. 3 DTG curves of CuCoZnAl-LDHs. The data collected in air and N_2 atmosphere are represented by solid and dotted lines, respectively.

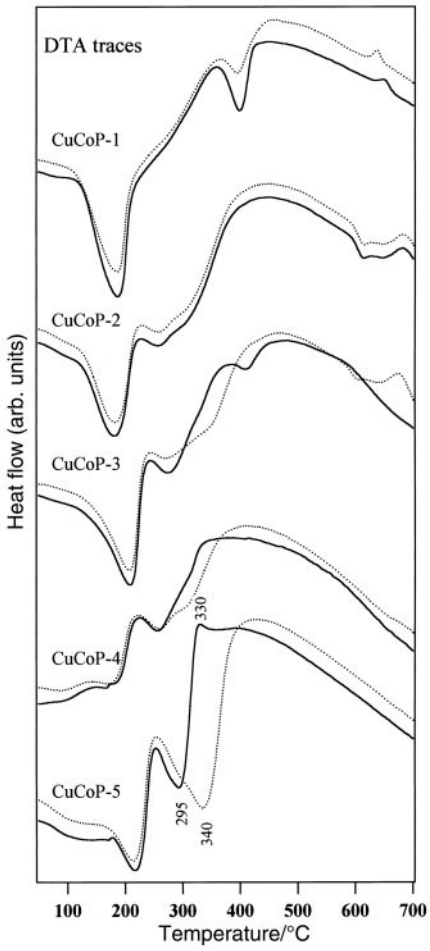

Fig. 4 Differential thermal analysis traces of CuCoZnAl-LDHs. The data collected in air and N_2 atmosphere are represented by solid and dotted lines, respectively.

These results infer that the oxidation of Co^{2+} to Co^{3+}, presumably an exothermic process, takes place in the same temperature range as that of the endothermic decomposition of interlayer CO_3^{2-} anions and the hydroxyl layer in the T_2 region. As a consequence, the endothermic effect of T_2 is cancelled out by the exothermic effect and hence the T_2 process appears as a weak endotherm. This result is in accordance with the results obtained by many other researchers in the thermal decomposition of various Co-based LDH systems.[22,30,31,35]

Temperature programmed reduction (TPR). The reducibility of copper and cobalt cations in the LDH matrix as well as in the mixed oxides was followed by TPR experiments. The TPR profiles of all the uncalcined samples are shown in Fig. 5. It should be remembered that, during TPR runs, the LDH structure of the present system is being destroyed while Cu^{2+} and Co^{2+} cations in the layer are reduced to their metallic states. It is, however, assumed that both Zn^{2+} and Al^{3+} are not reduced under the experimental conditions employed. CuCoP-1 containing Cu without Co exhibits a doublet with the maximum rate of H_2 consumption occurring at *ca.* 235 and 290 °C. Under our experimental conditions, pure CuO (Wako Chemicals, Japan) exhibited a single peak with a maximum rate of H_2 consumption at *ca.* 320 °C. Thus, the H_2 consumption observed for CuCoP-1 in this region should correspond to the reduction of Cu^{2+} present in the brucite-like layer of the LDH. The appearance of a doublet may be due to the existence of Cu^{2+} ions in two slightly different chemical environments. However, a recent study, using TPR followed by mass spectrometry, of some of the CuAl-LDH precursors revealed that the reduction of residual NO_3^- anions into NO takes place around 230 °C and that the reduction of Cu^{2+} starts when practically all the NO_3^- anions have been decomposed.[32] In order to check if the reduction of NO_3^- anions contributes to the H_2 consumption in these samples, the quantity of H_2 consumed was calculated from the integrated peak areas. The ratio of the amount of H_2 consumed to the Cu + Co contents [H_2/(Cu + Co) mol/mol] is included in Fig 5, which shows that the ratio is close to 1.0 (within the experimental error of *ca.* 10%). From these results, it appears that in our system the contribution to H_2 consumption in TPR due to the reduction of NO_3^- anions to NO is insignificant and that the doublet is mainly due to the existence of Cu^{2+} cations in more than one chemical environment. This point will be further substantiated from the TPR of samples calcined at 300 °C, which will show a similar intense doublet, although the XRD results will show the formation of a poorly crystallized CuO phase (*vide infra*). It should be recalled that the XRD of the uncalcined sample indicated the presence of MT together with the LDH phase. Hence, it is possible that the reduction of Cu^{2+} ions in this multiphasic system occurs at different temperatures. Sample CuCoP-5 containing Co without Cu exhibits a broad H_2 consumption band from 350 to 700 °C with the maximum rate of H_2 consumption centered around 470 °C. The H_2/Co stoichiometry is very close to unity, indicating the reduction of all the Co^{2+} ions present in the LDH framework. This result is in contrast to that observed in our earlier study on the TPR of the CoAl-LDH system, wherein the reduction of Co was incomplete even up to 700 °C.[31] This difference in the reducibility of Co^{2+} ions is due to the difference in the Al content in the sample, because it is very well known that the presence of Al greatly impedes the reducibility of Co species.[36] The TPR of the samples containing both Cu^{2+} and Co^{2+} with different Cu^{2+}/Co^{2+} ratios shows in general that the position of the H_2 consumption peak corresponding to Cu^{2+} shifts toward lower temperature with increasing Co content up to CuCoP-3. This demonstrates that the reducibility of Cu^{2+} is enhanced by the substitution of some Cu^{2+} by Co^{2+} in the LDH framework. On the other hand, the effect of copper concentration on the reducibility of Co^{2+} is not apparent, as the TPR peaks for the reduction of Co^{2+} are not distinguishable from that of Cu^{2+}. CuCoP-4, which contains relatively lower amounts of Cu^{2+}, shows a peak around 295 °C together with a sharp peak at *ca.* 470 °C.

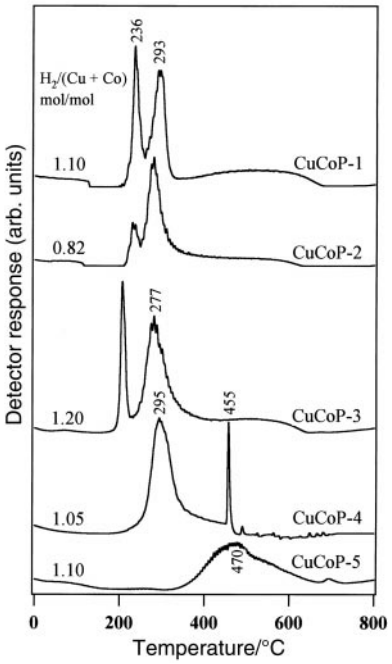

Fig. 5 Temperature programmed reduction profiles of CuCoZnAl-LDHs.

Characterization of mixed oxides

XRD. The structural transformations occurring during thermal decomposition of CuCoZnAl-LDHs at different temperatures and their redox properties were investigated systematically using XRD and TPR. In order to understand the effect of Co on the crystalline phases formed during thermal decompostion of these materials three samples were selected, *viz.* (i) CuCoP-1, without Co, (ii) CuCoP-5, without Cu, and (iii) CuCoP-3 containing both Cu and Co with a Cu/Co atomic ratio around 1 for calcination study. For the sake of better understanding, the XRD and TPR results of these materials are discussed in the same order.

The XRD patterns of CuCoP-1 calcined at different temperatures are shown in Fig. 6. Calcination at 300 °C results in the destruction of the layered structure and the formation of a poorly crystallized tenorite (CuO)-like phase. Other phases containing Zn and Al may be present in their amorphous state as no XRD lines other than CuO can be detected. Increase in calcination temperature improves the crystallinity of the CuO phase together with the crystallization of Zn and Al containing phases. Thus, a mixture of CuO and ZnO phases is detected in the sample calcined at 450 °C. Further calcination at 700 and 900 °C results in the formation of a cubic spinel phase similar to that of $CuAl_2O_4$ or $ZnAl_2O_4$ in addition to the CuO and ZnO phases. Interestingly, the CuO phase seems to be predominant at all the calcination temperatures. The formation of a Zn-containing CuO solid solution during calcination of Cu–ZnO methanol synthesis catalysts is known in the literature.[37] In order to check this, the *d* parameters of the (−111) and (200) planes (the most intense lines) have been calculated. It can be seen from Table 3 that *d*(−111) is in the range 2.521 to 2.523 Å, which is very close to the literature value (2.524 Å). In contrast, *d*(200) is in the range 2.320 to 2.325 Å, which is slightly higher than the literature value (2.311 Å). Taking into account the tetrahedral ionic radii of Cu^{2+} (0.57 Å) and Zn^{2+} (0.60 Å)[26] the minor increase in *d*(200) with respect to the literature value

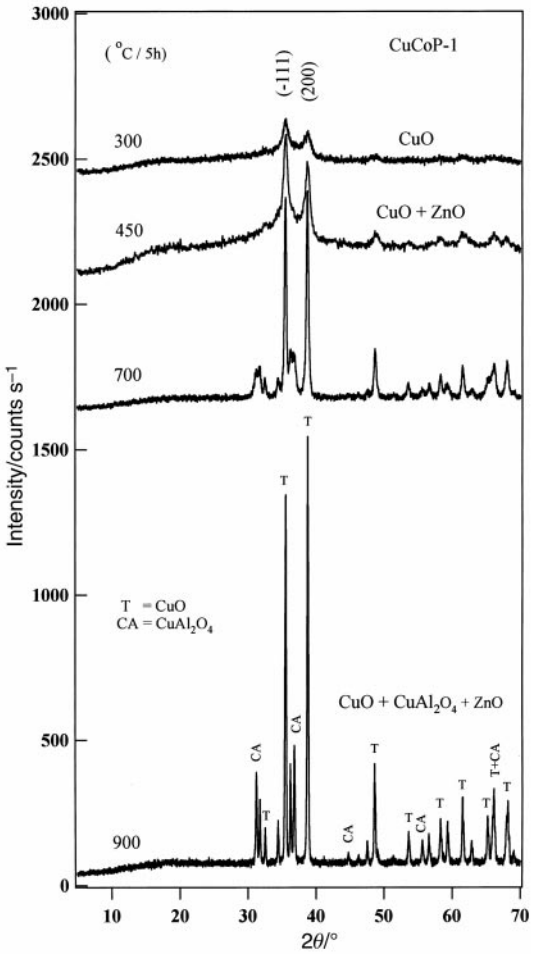

Fig. 6 X-Ray powder diffraction patterns of CuCoP-1 calcined at different temperatures. The crystalline phases identified are marked in the spectrum of the sample calcined at 900 °C. The unmarked peaks correspond to ZnO phase.

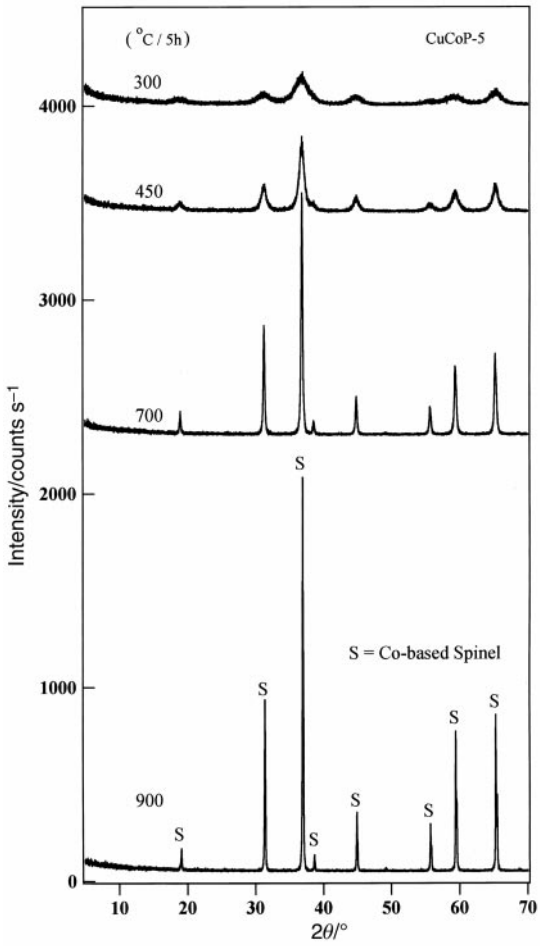

Fig. 7 X-Ray powder diffraction patterns of CuCoP-5 calcined at different temperatures. The crystalline phases identified are marked in the spectrum of the sample calcined at 900 °C.

is likely to be due to the dissolution of Zn preferentially in the (200) plane of the CuO. Since XRD lines corresponding to the spinel phase are discerned well only in the sample calcined at 900 °C, the lattice parameter '*a*' of the spinel phase was calculated from the *d*(311), *d*(220), *d*(440) and *d*(511) and it corresponds to 8.085 Å. This value is very close to those of $CuAl_2O_4$ (8.075 Å; JCPDS file No. 33-448) and $ZnAl_2O_4$ (8.086 Å; JCPDS file No. 5-0669) and hence it is difficult to ascertain the nature of the spinel phase formed. However, taking into account the facts that the ZnO phase still exists in the sample and that the Al/Zn atomic ratio in the precursor is *ca.* 1.3 (see Table 1), which is less than the stoichiometric ratio (Al/Zn = 2) required for the formation of $ZnAl_2O_4$ spinel, we attribute the spinel phase to $CuAl_2O_4$ rather than $ZnAl_2O_4$. This assumption will be further substantiated by our TPR results (*vide infra*), which will show H_2 consumption bands at high temperatures, very close to that that observed in the $CuAl_2O_4$ spinels.

Table 3 Lattice parameters of tenorite (CuO) phase obtained by the calcination of CuCoP-1 at different temperatures

	d parameter/Å at different calcination temperatures			
Plane	450 °C	700 °C	900 °C	Literature value (tenorite)[a]
(−111)	2.521	2.523	2.523	2.524
(200)	2.325	2.322	2.320	2.311

[a]JCPDS file No. 41-254.

Fig. 7 displays the XRD patterns of Co-rich CuCoP-5 without Cu calcined at different temperatures. In contrast to that observed in the thermal decomposition of CuCoP-1, the XRD of CuCoP-5 exhibits a spinel-like phase (Co-based spinel) even at 300 °C. No XRD lines corresponding to rocksalt-type CoO can be detected although the formation of CoO phase during calcination, under N_2 atmosphere, of some of the Co-based precursors has been reported.[38] The formation of a spinel phase in the present study even at low temperature is not surprising as the sample was calcined under static air atmosphere. Also, CoO is thermodynamically less stable compared to other co-based spinels in intermediate temperatures (for example, CoO: $\Delta G^\circ_f = -214$ kJ (mol Co)$^{-1}$; Co_3O_4: $\Delta G^\circ_f = -258$ kJ (mol Co)$^{-1}$). The intensity of the XRD lines increases with increasing calcination temperature implying that the crystallinity of the spinel phase improves. The sample calcined at 900 °C develops additional shoulders for peaks recorded at higher 2θ angles indicating the crystallization of an additional spinel phase. Taking into account the chemical composition of the starting material (Co : Zn : Al atomic ratio = 2.27 : 0.81 : 1) and also that the samples were calcined in static air atmosphere, one would expect the formation of Co_3O_4, $CoAl_2O_4$, Co_2AlO_4, $ZnCo_2O_4$ and $ZnAl_2O_4$ spinels during thermal decomposition of this compound. However, the lattice constants of these spinels are comparable to each other (see Table 4). The '*a*' parameters of the spinel phase obtained by the calcination of the precursor at 450, 700 and 900 °C are 8.080, 8.083 and 8.067 Å, respectively. The '*a*' parameter of the shoulder peaks recorded for the sample calcined at 900 °C is 8.057 Å. These values are very close to those of all the possible spinel phases mentioned above. A closer inspection of the

Table 4 Lattice parameters of spinel phases obtained by the calcination of CuCoP-5 at different temperatures

Calcination temperature/°C	Observed '*a*' parameter/Å	Literature data	
		Spinel phase	'*a*' parameter/Å
450	8.080	Co_3O_4	8.084[a]
700	8.083	$CoAl_2O_4$	8.103[b]
900	8.067	Co_2AlO_4	8.086[c]
	8.057	$ZnCo_2O_4$	8.095[d]
		$ZnAl_2O_4$	8.085[e]

[a]JCPDS file No. 42-1467. [b]JCPDS file No. 10-458. [c]JCPDS file No. 38-814. [d]JCPDS file No. 23-1390. [e]JCPDS file No. 5-0669.

relative intensities of the XRD lines and their '*d*' values revealed the formation of either Al- and Zn-containing Co_3O_4 solid solutions or Al-containing $ZnCo_2O_4$ solid solution or a mixture thereof during calcination of these materials in the temperature range investigated. Baird and coworkers have reported the formation of an Al- and Zn-containing solid solution of Co_3O_4 during thermal decomposition of a CoZnAl-hydroxycarbonate precursor with a Co : Zn : Al atomic ratio of 2.4 : 0.6 : 1.0 around 450 °C.[39] However, they have not reported the nature of the phases formed at higher calcination temperatures. Our TPR study (*vide infra*) will show evidence for the formation of a Zn- and Al-containing Co_3O_4 solid solution and/or an Al-containing $ZnCo_2O_4$ solid solution during calcination of these samples.

The XRD patterns of CuCoP-3, which contains both Cu and Co with a Cu/Co atomic ratio very close to 1, are shown in

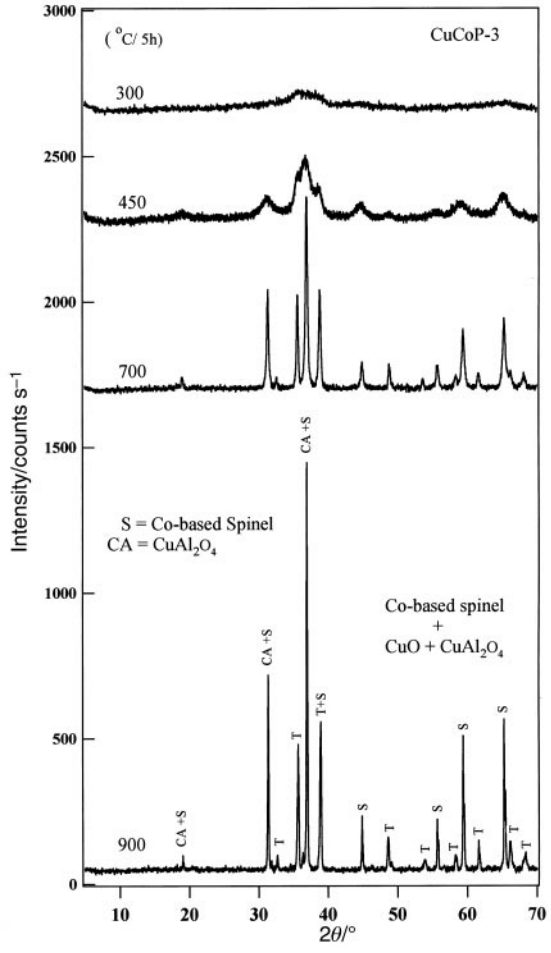

Fig. 8 X-Ray powder diffraction patterns of CuCoP-3 calcined at different temperatures. The crystalline phases identified are marked in the spectrum of the sample calcined at 900 °C. The shoulders at higher 2θ angle correspond to $CuAl_2O_4$ spinel.

Table 5 Lattice parameters of CuO and spinel phases obtained by the calcination of CuCoP-3 at different temperatures

Calcination temperature/°C	Crystalline phase	Lattice parameter/Å	
450	CuO	*d*(−111)	2.517
		d(200)	2.330
	Spinel	'*a*'	8.113
700	CuO	*d*(−111)	2.519
		d(200)	2.320
	Spinel	'*a*'	8.076
900	CuO	*d*(−111)	2.516
		d(200)	2.313
	Spinel	'*a*'	8.063
			8.073

Fig. 8. It can be seen that calcination of CuCoP-3 at 300 °C results in the destruction of the layered structure and formation of a poorly crystallized phase whose crystallinity improves with increasing calcination temperature. Peaks corresponding to a mixture of CuO and Co-based spinel are clearly identified in the sample calcined at 450 °C and above. However, in contrast to what was observed in CuCoP-1, the ZnO phase is not detected. Similar to what was observed in the calcination of CuCoP-5, additional shoulders at higher 2θ angles are also noticed in the sample calcined at 900 °C. A closer inspection of the XRD pattern and the '*d*' parameters revealed that these shoulders correspond to $CuAl_2O_4$ spinel. The lattice parameters of the CuO and the Co-based spinel phases calculated from the XRD data are summarized in Table 5. Unlike what was observed in CuCoP-1, the '*d*' parameters of CuO phase varies for the samples calcined only up to 700 °C. For the sample calcined at 900 °C, *d*(−111) and *d*(200) are very close to the literature values (see Table 3 and Table 5). The '*a*' parameter of the observed spinel phase is in close agreement with those observed in CuCoP-5. Thus, from these results the crystalline phases formed upon calcination of CuCoP-3 are a combination of those phases observed in CuCoP-1 and CuCoP-5 except ZnO. It should be recalled that ZnO was not observed even in CuCoP-5. The absence of a separate ZnO phase in the Co-containing LDHs supports our hypothesis on the formation of Zn-containing Co-based spinels such as $ZnCo_2O_4$. This spinel phase is known to be formed at a temperature of around 450 °C.[22] Morpurgo *et al.*[21] have also reported the possibility of the formation of $ZnCo_2O_4$ spinel upon calcination of a similar CuCo-based LDH system.

TPR. The TPR profiles of CuCoP-1 calcined at different temperatures are shown in Fig. 9. In all cases, a major reduction is recorded in the temperature range between 200 and 300 °C, which can be attributed to the reduction of CuO species generated during calcination of the precursors. However, the calcination temperature significantly influences the shape and bandwidth of the profiles. The sample calcined at 300 °C exhibits a broad doublet, which is similar to that recorded in the uncalcined sample (see Fig. 5) The peak becomes sharper as the calcination temperature increases. A shoulder around 300 °C is also noticed for the sample calcined at 700 °C, whose intensity further increases and shifts to *ca.* 320 °C when the specimen is calcined at 900 °C. Apart from these sharp reduction peaks, a broad component between 400 and 700 °C can also be observed in all cases. The sample calcined at 700 °C develops an additional broad peak around 725 °C. It can be inferred from these results that depending upon the calcination temperature, several reducible Cu^{2+} species are generated. The existence of well dispersed CuO (isolated Cu^{2+}), clustered Cu^{2+}, surface $CuAl_2O_4$, bulk $CuAl_2O_4$ *etc.* is known in CuAl and CuZnAl mixed oxide systems, wherein the Cu^{2+} species are reduced at different temperatures.[14,40] Generally, the Cu^{2+} ions interacting with Al^{3+} are reduced relatively at higher

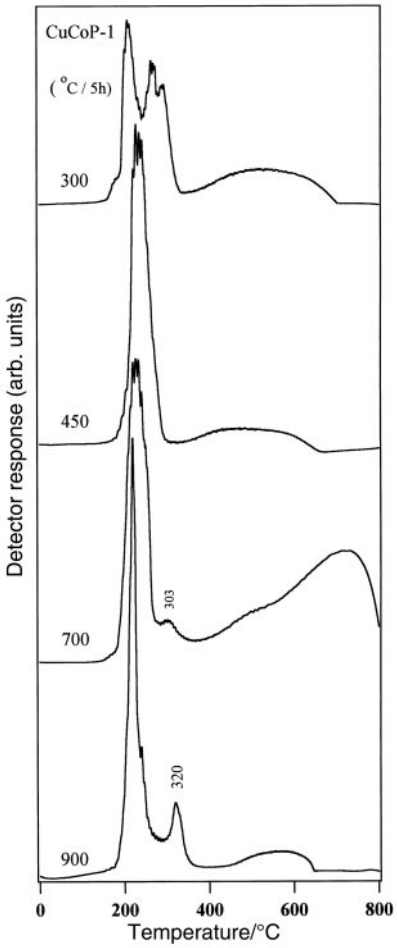

Fig. 9 Temperature programmed reduction profiles of CuCoP-1 calcined at different temperatures.

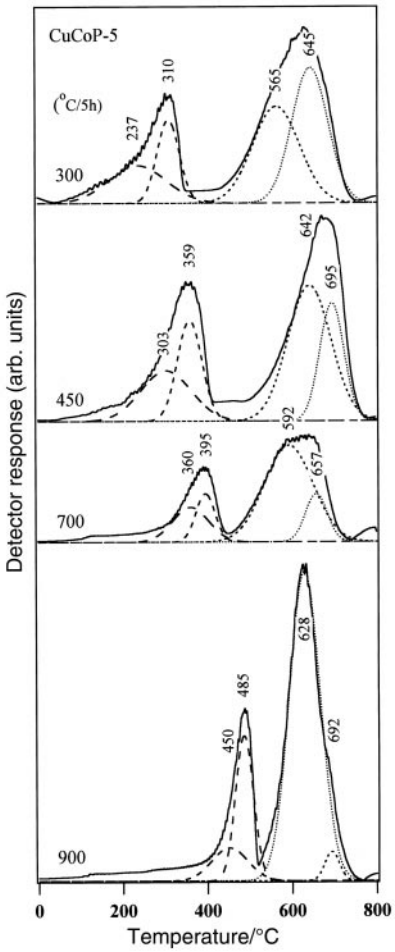

Fig. 10 Temperature programmed reduction profiles of CuCoP-5 calcined at different temperatures. Solid lines are original curves and dotted lines are deconvoluted curves.

temperature, because the Al^{3+} ion polarizes the covalent Cu–O bonds thereby increasing the effective charge of the copper ions. As a consequence, the lattice energy increases resulting in an increase in the TPR reduction temperature. Our thermal analyses and XRD data indicated that the layered structure was collapsed at 300 °C and formed a poorly crystallized CuO phase. Since amorphous Zn- and Al-containing phases, possibly ZnO and Al_2O_3, are expected to be present at this temperature, it is likely that the CuO phase is dispersed on the amorphous ZnO and Al_2O_3 phases. The interaction of Cu^{2+} species with these amorphous phases with different strengths would lead to the reduction of Cu^{2+} at different temperatures. However, at higher calcination temperatures, because of the structural ordering, the CuO is reduced sharply in a single step. It should be noted that the maximum rate of H_2 consumption for CuO obtained by calcination of the precursor is (*ca.* 230 °C) less than that of pure CuO (*ca.* 320 °C) probably because of the dispersion of CuO on the ZnO support. Since the crystallinity of CuO and $CuAl_2O_4$ spinel phases is improved greatly, the shoulder at *ca.* 300 °C for the sample calcined at 700 and 900 °C may be due to the reduction of clustered CuO species or Cu^{2+} interacting with the Al^{3+} cations (surface $CuAl_2O_4$ spinel).[14,40] The broad component observed between 400 and 700 °C can be attributed to the reduction of Cu^{2+} species of $CuAl_2O_4$ spinel as a similar high temperature reduction peak has been observed in TPR of $CuAl_2O_4$ spinels prepared by different methods.[40–42]

Fig. 10 presents the TPR profiles of CuCoP-5 calcined at different temperatures. It can be seen that, in all cases, two reduction regions, one between 200 and 500 °C and the other above 500 °C, are observed. While the position of the first peak shifts significantly toward higher temperature with increasing calcination temperature, there is no regular trend in the position of the second peak although peaks in both the regions become sharper with increasing calcination temperature. Since the shapes of the peaks are not symmetrical and possess shoulders, attempts have been made to deconvolute the original profiles. Thus, each main peak has been deconvoluted into two peaks. The quantitative data derived from the deconvolution are collected in Table 6. The results suggest that there exist at least four kinds of Co species in these samples. For the specimen calcined at 300 °C, the maximum rate of H_2 consumption corresponds to the first reduction region which appears at 237 and 310 °C (peak 1 and peak 2, respectively), while that for the second reduction region appears at 565 and 645 °C (peak 3 and peak 4, respectively). It should be mentioned that the reference samples of both CoO (Co species in +2 oxidation state) and Co_3O_4 (cobalt in both +2 and +3 oxidation states) are also reduced in the first reduction region.[31] On the other hand, pure $CoAl_2O_4$ (tetrahedrally coordinated Co^{2+} with Al^{3+} neighbors) is reduced in the second reduction region above 700 °C. Hence,

Table 6 Quantitative TPR data of CuCoP-5 calcined at different temperatures

Calcination temperature/°C	Peak position/°C and its contribution (%)			
	Peak 1	Peak 2	Peak 3	Peak 4
300	237 (16)	310 (14)	565 (34)	645 (36)
450	303 (19)	359 (18)	642 (43)	695 (20)
700	360 (16)	395 (12)	592 (59)	657 (13)
900	450 (9)	485 (19)	628 (69)	692 (3)

as pointed out for the reducibility of copper, the presence of Al greatly impedes the reducibility of Co species as well.[36] Therefore, peaks in the first reduction region should correspond to the reduction of Co_3O_4-like species or $ZnCo_2O_4$ spinel (Co species without Al^{3+} neighbors). On the other hand, peaks recorded in the second reduction regions are due to the reduction of $CoAl_2O_4$-like species or Al-containing Co_3O_4/$ZnCo_2O_4$ solid solutions (Co^{2+} species with Al^{3+} neighbors). It should be remembered that the existence of two kinds of spinel species is undistinguishable by the XRD while they can be realized by TPR. The maximum rate of H_2 consumption corresponds to the first reduction region, it increases with increasing calcination temperature and approaches the second peak. This result can be attributed to the dissolution of more and more Al^{3+} cations in the Co_3O_4-like spinel or $ZnCo_2O_4$ spinel species and transformation to $CoAl_2O_4$-like spinel with increasing calcination temperature. This is in line with our XRD, which showed additional shoulders for the sample calcined at 900 °C and indicated the formation of mixed spinel phases (see Fig. 7 bottom). Thus, at higher calcination temperatures, a mixture of Co_3O_4-like or $ZnCo_2O_4$ spinel together with $CoAl_2O_4$-like spinel phases is formed. Similar results have been observed in our earlier study on the TPR characterization of materials derived from CoAl-LDHs and also by other researchers in the TPR characterization of some Co-based mixed oxides.[31,36,43]

The TPR profiles of CuCoP-3 containing both Cu and Co calcined at different temperatures are shown in Fig. 11. It can be seen that, for the samples calcined between 300 and 700 °C, the H_2 consumption due to the reduction of Cu^{2+} species of CuO is recorded around 200 °C, which is very close to that observed in CuCoP-1. However, the bandwidth and the intensity of the profiles are relatively less compared to those observed in the CuCoP-1, because the Cu content in CuCoP-3 is only about half that of CuCoP-1 (see Table 1). Another broad reduction peak, whose intensity and peak maximum increase with increasing calcination temperature, is also observed on the high temperature side. Since the position of this peak is similar to that observed in the first reduction region of CuCoP-5 calcined at different temperatures (see Fig. 10), this peak can be assigned to the reduction of Co_3O_4-like spinel or $ZnCo_2O_4$. The reducibility of Co species is diminished with increasing calcination temperature. This is because of the dissolution of more Al^{3+} cations in the spinel similar to that occurring in the materials derived from CoZnAl-LDH without Cu (CuCoP-5). The sample calcined at 900 °C exhibits two broad peaks, one between 200 and 400 °C and the other between 500 and 700 °C with maximum rates of H_2 consumption occurring around 250, 380 and 625 °C. It should be recalled that the XRD of the sample indicated the formation of a mixture of CuO, $CuAl_2O_4$ together with Co_3O_4-like/Al-containing $ZnCo_2O_4$ spinel. Thus, the broad component in the low temperature region can be attributed to the reduction of Cu^{2+} species present in the CuO and $CuAl_2O_4$ spinel, while that in the higher temperature region can be assigned to the reduction of Co species present in the Al-containing $ZnCo_2O_4$ spinel. Note that the TPR of CuCoP-1 calcined at 900 °C showed an intense peak around 220 °C for the reduction of CuO species (see Fig. 10). In contrast, the intensity of this peak is significantly decreased and the peak is shifted toward higher temperature in the CuCoP-3 analogue. The decrease in the reducibility of CuO is probably because of the dissolution of Al^{3+} and the formation of $CuAl_2O_4$ spinel as evidenced from the XRD pattern.

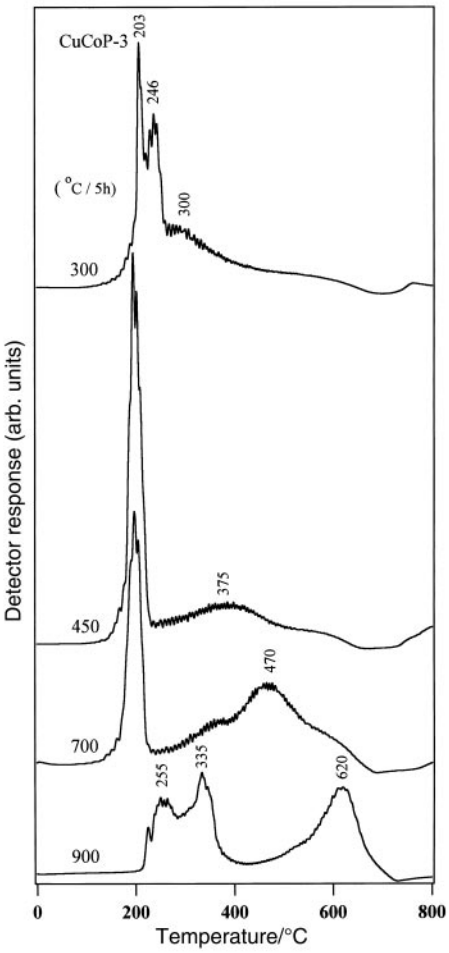

Fig. 11 Temperature programmed reduction profiles of CuCoP-3 calcined at different temperatures.

Comparison of CuCoZnAl-LDHs calcined at 450 °C

XRD, TPR and UV–Vis DRS. The LDH materials calcined around 450 °C are generally being employed as catalysts in a variety of reactions.[1,7–9,11–14] In fact, we are currently investigating the catalytic performance of these materials calcined at 450 °C in the oxidative steam reforming of methanol for H_2 production. In order to understand the effect of Co substitution on the structural and redox properties of CuCoZnAl-multicomponent mixed oxide catalysts, the XRD, UV–Vis DRS and TPR results of all the precursors calcined at 450 °C (CuCoC-1 to CuCoC-5) are compared in Fig. 12, 13 and 14, respectively. It can be noted from Fig. 12 that Cu-rich CuCoC-1 exhibits a diffraction pattern corresponding to a mixture of CuO and ZnO phases. The crystallinity of these phases decreases with a consequent improvement in the crystallinity of the spinel phase with decreasing Cu content or increasing Co content. Co-rich CuCoC-5 exhibits a relatively well-crystallized Co-based spinel phase. Thus, the catalysts derived from intermediate compositions contain both CuO and Co-based spinel phases. The existence of such a mixed oxide phase is expected to bring about an interaction between them, which would alter the physicochemical properties of the catalysts.

The UV–vis DRS spectra of all the samples calcined at 450 °C are depicted in Fig. 13. Upon comparison of results in Fig. 13 with those in Fig. 2, one can notice that the destruction of the layered structure and the formation of poorly crystallized mixed oxides upon calcination at 450 °C produces relatively strong bands compared to their uncalcined counterparts (compare Fig. 2 and Fig. 13). The CuCoC-1 without Co exhibits bands at *ca.* 300, 380 and 650 nm together with a shoulder around 250 nm. The band around 650 nm corresponds to the $^2E_g \rightarrow {}^2T_{2g}$ transition of Cu^{2+} ions in the CuO phase. However, the observed shift from *ca.* 800 nm for the CuO reference sample (see Fig. 2) to *ca.* 650 nm and the broadness of the band suggest a significant distortion in the

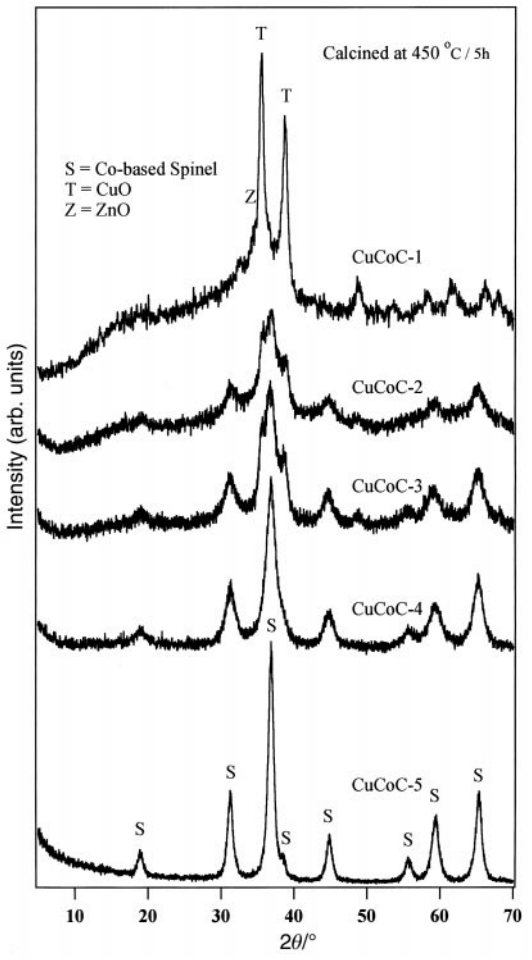

Fig. 12 X-Ray powder diffraction patterns of CuCoZnAl-LDHs calcined at 450 °C.

symmetry of the copper environment, probably because of the interaction of Cu^{2+} ions with the ZnO and amorphous Al_2O_3 phases.[14] The band around 380 nm, which is not observed clearly in the uncalcined sample, is due to the zinc–oxygen charge transfer band of ZnO. The bands between 250 and 300 nm are attributed to the charge transfer involving Cu^{2+}–O^{2-}–Cu^{2+} species, possibly like a cluster or bulk-like species.

The spectrum of CuCoC-5, without Cu, exhibits strong bands at *ca.* 670, 400 and 250 nm. These bands are very close to those observed for the Co_3O_4 reference and are assigned to the $^1A_{1g}$ (I) → $^1T_{1g}$ (I), $^1A_{1g}$ (I) → $^1T_{2g}$ (I) and O_2^{2-} → Co^{3+} (oh) LMCT transitions, respectively (see Table 2). The observed results are in line with the XRD results, which indicated the formation of a Zn- and Al-containing Co_3O_4 solid solution or $ZnCo_2O_4$ spinel upon calcination at this temperature. The other samples containing both Cu and Co exhibit bands at *ca.* 670, 400 and 260 nm. These bands are similar to those observed in the CuCoC-1 and CuCoC-5 samples and hence are attributed to the Cu^{2+} in CuO and Co^{3+} in Co_3O_4-like spinel phases. However, there is an initial decrease in the overall intensity or Kubelka–Munk function until CuCoC-3 and then the intensity increases with increasing Co content. This is may be due to the decrease of crystallinity of the mixed oxide phases formed until CuCoC-3 as evidenced from their XRD patterns (see Fig. 12). It should also be noted that the band corresponding to the LMCT of ZnO, which appears around 380 nm in CuCoC-1, is absent in the Co-containing samples. This supports our XRD data on the absence of the ZnO phase in the calcined materials and suggests the formation of a Zn-containing Co_3O_4 solid solution or $ZnCo_2O_4$ spinel consistent with our XRD data and literature reports.[21,22]

Fig. 14 depicts the TPR profiles of all the samples calcined at 450 °C. It can be clearly seen that the maximum rate of H_2 consumption corresponds to the reduction of the CuO phase around 200 °C shifts gradually toward lower temperature (from

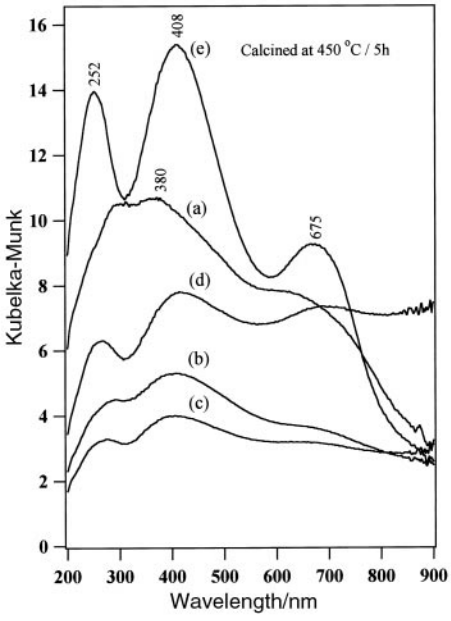

Fig. 13 Ultraviolet–visible diffuse reflectance spectra of CuCoZnAl-LDHs calcined at 450 °C. (a) CuCoC-1, (b) CuCoC-2, (c) CuCoC-3, (d) CuCoC-4 and (e) CuCoC-5.

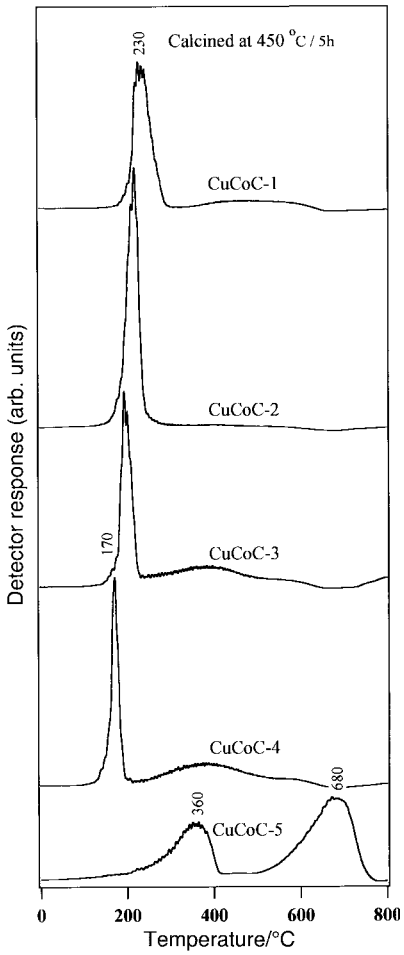

Fig. 14 Temperature programmed reduction profiles of CuCoZnAl-LDHs calcined at 450 °C.

around 230 °C for CuCoC-1 to around 170 °C for CuCoC-4). This result implies that the substitution of Co^{2+} in the CuZnAl-LDH framework favours the reducibility of Cu^{2+}. It should be remembered that such an improvement in the Cu reducibility with increasing Co content is less significant in the uncalcined samples (see Fig. 5). The H_2 consumption due to the reduction of Co in Co_3O_4-like spinel on the high temperature side is very weak for the sample CuCoC-2 containing very low amounts of Co (see Table 1). The intensity of this peak around 380 °C increases with increasing Co content and it appears at *ca.* 360 °C for the sample CuCoC-5. Thus, although the changes in the peak positions corresponding to the reduction of Co in the Co_3O_4-like spinel or $ZnCo_2O_4$ are not clearly discernable, the results indicate in general that the reducibility of Co is diminished to some extent with increasing Cu content in the sample. The peak around 675 °C for the reduction of Co species in the Al-containing Co-based spinel is recorded only in the Co-rich CuCoC-5 while it appears as a small shoulder around 600 °C in CuCoC-3 and CuCoC-4. In brief, while the reducibility of Cu species is enhanced with increasing cobalt content, the reducibility of Co species is diminished with increasing copper content. This phenomenon clearly indicates the operation of a sort of Cu–Co redox mechanism in these materials. This also reveals the existence of a synergetic interaction between copper and cobalt species. The existence of a Cu–Co synergistic interaction was believed to be responsible for the oxygenate formation in the conversion of synthesis gas to methanol and higher alcohols over similar CuCoZnAl-multicomponent mixed oxide catalysts.[16,17] Further studies using X-ray photoelectron spectroscopy (XPS) and high energy X-ray absorption spectroscopy (XANES/EXAFS) are currently under way in order to thoroughly understand the Cu–Co interaction in these interesting catalytic materials.

Conclusions

The coprecipitation of mixed metal nitrates of Cu, Co, Zn and Al produces well-crystallized hydrotalcite (HT)-like layered double hydroxides (LDHs) with a general formula: $[Cu_{1-(x+y+z)}Co_xZn_yAl_z(OH)_2]^{z+}[(CO_3^{2-})_{z/2}{\cdot}mH_2O]^{z-}$, wherein all the metal ions exist in the octahedral brucite-like layer. The structural properties and the reducibility of as-synthesized as well as calcined samples are influenced greatly by the Cu/Co atomic ratio. The Cu-rich sample produces malachite $[Cu(OH)_2CO_3]$ as an impurity because of the operation of the Jahn–Teller effect. The crystallinity of the material decreases with increasing Co content. The introduction of Co in the CuZnAl-LDH system decreases the decomposition temperature because of its ability to form thermodynamically stable spinel phases even at low temperatures. Calcination of the Cu-rich sample produces a mixture of CuO, ZnO and a Zn-containing $CuAl_2O_4$ spinel solid solution. On the other hand, the Co-rich sample, without Cu, produces an Al-containing Co_3O_4 solid solution and/or $ZnCo_2O_4$ spinel. The material containing both Cu and Co produces, depending on the calcination temperature, all those phases (except ZnO) observed in the Cu-rich as well as in the Co-rich samples. The reducibility of Cu and Co species of the calcination products are influenced by the nature of the phases formed. For the samples calcined at 450 °C, the reducibility of Cu^{2+} of the CuO phase is significantly improved with increasing Co content while a reverse effect is noted for the reducibility of Co with increasing Cu content. The existence of a sort of Cu–Co synergistic interaction probably originated by the intimate contact and by the good interdispersion of the oxide phases formed has been noticed.

Acknowledgements

The authors would like to express their sincere gratitude to Dr. Akihiko Nakatsuka, Department of Advanced Materials Science and Engineering, Yamaguchi University, Japan for the generous gift of the $CoAl_2O_4$ reference sample. Thanks are also due to Dr. M. Suzuki, who is presently at the Geological Survey of Japan, Tsukuba, and Dr. Osaki of our institute for their help in many ways during this study. One of the authors (S. V.) is grateful to the Japan Science and Technology Corporation (JST) for financial assistance through the Cooperative System for Supporting Priority Research.

References

1 F. Cavani, F. Trifiro and A. Vaccari, *Catal. Today*, 1991, **11**, 173.
2 A. de Roy, C. Forano, K. El Malki and J-P. Besse, in *Synthesis of Microporous Materials, Vol.2, Expanded Clays and Other Microporous Systems*, ed. M. L. Occelli and H. E. Robson, Van Nostrand Reinhold, New York, 1992, p. 108.
3 *Recent Catalytic Applications of Hydrotalcite-type Anionic Clays*, ed. D. Tichit and A. Vaccari, *Appl. Clay Sci.,* 1998, vol. 13, p. 311
4 S. P. Newman and W. Jones, *New J. Chem.*, 1998, **22**, 105.
5 V. Rives and M. A. Ulibarri, *Coord. Chem. Rev.*, 1999, **181**, 67.
6 J. Choy, S. Kwak, Y. Jeong and J. Park, *Angew. Chem., Int. Ed.*, 2000, **39**, 4042.
7 S. Kannan, C. S. Swamy, Y. Li, J. N. Armor and T. A. Braymer, *US Pat.*, 5407652, 1995.
8 A. Bhattacharyya, *US Pat.*, 9903779, 1999.
9 J. S. Valente, F. Figueras, M. Gravelle, P. Kumbhar, J. Lopez and J.-P. Besse, *J. Catal.*, 2000, **189**, 370.
10 M. J. L. Ginés, N. Amadeo, M. Laborde and C. R. Apesteguía, *Appl. Catal. A: General*, 1995, **131**, 283.
11 S. Velu, K. Suzuki and T. Osaki, *Catal. Lett.*, 1999, **62**, 159.
12 S. Velu, K. Suzuki and T. Osaki, *Catal. Lett.*, 2000, **69**, 43.
13 S. Velu, K. Suzuki and T. Osaki, *Chem. Commun.*, 1999, 2341.
14 S. Velu, K. Suzuki, M. Okazaki, M. P. Kapoor, T. Osaki and F. Ohashi, *J. Catal.*, 2000, **194**, 373.
15 P. Courty, D. Durand, E. Freund and A. Sugier, *J. Mol. Catal.*, 1982, **17**, 241.
16 J. E. Baker, R. Burch and S. E. Golunski, *Appl. Catal.*, 1989, **53**, 279.
17 A. J. Marchi, J. I. Di. Cosimo and C. R. Apesteguía, *Catal. Today*, 1992, **15**, 383.
18 G. Fierro, M. L. Jacono, M. Inversi, R. Dragone and P. Porta, *Top.Catal.*, 2000, **10**, 39.
19 K. Zhu, C. Liu, X. Ye and Y. Wu, *Appl. Catal. A: General*, 1998, **168**, 365.
20 L. Yumin, L. Shetian, Z. Kaizhentg, Y. Xingkai and W. Yue, *Appl. Catal. A General.*, 1998, **169**, 127.
21 S. Morpurgo, M. L. Jacono and P. Porta, *J. Mater. Chem.*, 1994, **4**, 197.
22 P. Porta and S. Morpurgo, *Appl. Clay Sci.*, 1995, **10**, 31.
23 A. J. Marchi and C. R. Apesteguía, *Appl. Clay Sci.*, 1998, **13**, 35.
24 D. A. M. Monti and A. Baiker, *J. Catal.*, 1983, **83**, 323.
25 M. Del Arco, P. Malet, R. Trujillano and V. Rives, *Chem. Mater.*, 1999, **11**, 624.
26 R. D. Shannon, *Acta Crystallogr., Sect. A.*, 1976, **32**, 751.
27 Z. P. Xu and H. C. Zeng, *Chem. Mater.*, 2000, **12**, 2597.
28 B. C. Angeletti, F. Pepe and P. Porta, *J. Chem. Soc., Faraday Trans. 1*, 1977, **74**, 1972.
29 F. A. Cotton and G. Wilkinson, *Advanced Inorganic Chemistry*, 5th edn., John Wiley and Sons, New York, 1998, p. 730.
30 M. A. Ulibarri, J. M. Fernandez, F. M. Labajos and V. Rives, *Chem. Mater.*, 1991, **3**, 626.
31 S. Velu, K. Suzuki, M. P. Kapoor, S. Tomura, F. Ohashi and T. Osaki, *Chem. Mater.*, 2000, **12**, 719.
32 A. Alejandre, F. Medina, P. Salagre, X. Correig and J. E. Sueiras, *Chem. Mater.*, 1999, **11**, 939.
33 S. Velu and C. S. Swamy, *J. Mater. Sci. Lett.*, 1996, **15**, 1674.
34 V. Rives and S. Kannan, *J. Mater. Chem.*, 2000, **10**, 489.
35 M. Del Arco, R. Trujillano and V. Rives, *J. Mater. Chem.*, 1998, **8**, 761.
36 P. Arnoldy and J. A. Moulijn, *J. Catal.*, 1985, **93**, 38.
37 G. Sanker, S. Vasudevan and C. N. R. Rao, *J. Chem. Phys.*, 1986, **85**, 2291.
38 P. Porta, R. Dragone, G. Fierro, M. Inversi, M. L. Jacono and G. Moretti, *J. Chem. Soc., Faraday Trans.*, 1992, **88**, 311.

39 T. Baird, K. C. Campbell, P. J. Holliman, R. Hoyle, D. Stirling and B. P. Williams, *J. Chem. Soc., Faraday Trans.*, 1995, **91**, 3219.
40 F. Severino, J. L. Brito, J. Laine, J. L. G. Fierro and A. L. Agudo, *J. Catal.*, 1998, **177**, 82.
41 S. Sato, M. Iijima, T. Nakayama, T. Sodesawa and F. Nozaki, *J. Catal.*, 1997, **169**, 447.
42 M. Fernandez-Garcia, I. Rodriguez-Ramos, P. Ferreira-Aparicio and A. Guerrero-Ruiz, *J. Catal.*, 1998, **178**, 253.
43 S. Ribet, D. Tichit, B. Coq, B. Ducourant and F. Morato, *J. Solid State Chem.*, 1999, **142**, 382.